AAS 09-184

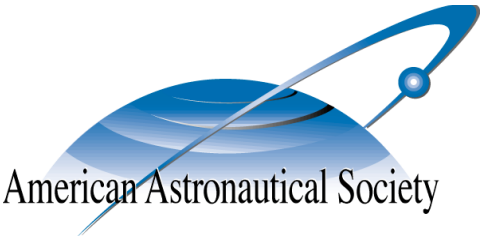

American Institute of
Aeronautics and Astronautics

ELECTROSTATIC SPACECRAFT COLLISION AVOIDANCE USING PIECE-WISE CONSTANT CHARGES

Shuquan Wang and Hanspeter Schaub

AAS/AIAA Spaceflight Mechanics Meeting

Savannah, Georgia **February 9-12, 2009**

AAS Publications Office, P.O. Box 28130, San Diego, CA 92198

(Preprint) AAS 09-184

ELECTROSTATIC SPACECRAFT COLLISION AVOIDANCE USING PIECE-WISE CONSTANT CHARGES

Shuquan Wang* **and Hanspeter Schaub†**

This paper develops a three-phase piece-wise constant spacecraft charge maneuver to achieve an short-range collision avoidance with a symmetric relative trajectory. This symmetric trajectory guarantees collision avoidance, restores the original relative motion direction, and keeps the relative change in kinetic energy level the same as the initial one. The paper first presents an analytical solution to calculate a unique symmetric trajectory when the middle phase is a circular trajectory. Next a general symmetric trajectory programming strategy is developed where the middle-phase can be any conic section. Four constraints are required to guarantee a symmetric collision avoidance trajectory, while five independent variables are required to solve the problem. This leaves one degree of freedom (DOF) which is utilized to optimize the trajectory subject to specific cost charge functions. There is a duality in the charge solution when solving for the open-loop trajectory with one of the solutions being false. This is addressed by properly initializing and confining the region of the numerical search routine. Minimum charge criteria are determined to avoid a collision by analyzing the geometric properties of the two-body system and comparing the results from circular transitional trajectory calculations.

INTRODUCTION

Clustered spacecraft have many advantages over a single large monolithic satellite. However, spacecraft cluster concepts also introduce the issue of potential collisions. In close-proximity spacecraft missions, such as close formations and small satellite swarms, the chance for spacecraft to collide must be treated carefully to prevent the huge cost of an unexpected collision. Collisions can occur when some spacecraft within the cluster have control or sensor failures, or are lacking in their guidance strategy to guarantee collision avoidance among a large number of cluster members. For long-term Earth-orbit missions, a collision can also occur when the influences of the orbital disturbances accumulate.

The most common approach in dealing with spacecraft collision avoidance is to examine the collision probability of a spacecraft cluster and perform some velocity corrections to reduce the probability to an acceptable level. Patera and Peterson in Reference 1 develop a method to select a maneuver that will reduce the collision probability. This method minimizes the maneuver magnitude and space vehicle propellant expenses. Slater et al. in Reference 2 use the available state and disturbance information to calculate the actual probability of collision based on a probabilistic model, and then discusses the velocity correction requirements to avoid collisions. In Reference 3, Patera proposes a spherical conflict volume to calculate the conflict probability in identifying high-risk conjunctions. The conflict probabilities are larger than associated collision probabilities and therefore are more easily interpreted. All of the above works use thrusters to achieve the velocity corrections. These strategies use propellent, which will increase the fuel budget of the spacecraft. Further, the associated exhaust plume impingement may cause damage to instruments on board when spacecraft are flying less than 100 meters apart.

In this paper a different scenario is considered where an active control strategy is used after a potential collision has been detected. The collision avoidance maneuver strategy uses only piece-wise constant electrostatic (Coulomb) forces. Coulomb thrusting can generate the required micro- and milli-Newton levels forces to avoid a collision of 2 slowly drifting spacecraft while requiring essentially no propellant and Watt-level of electrical power.

*Graduate Research Assistant, Aerospace Engineering Sciences Department, University of Colorado, Boulder, CO.
†Associate Professor, H. Joseph Smead Fellow, Aerospace Engineering Sciences Department, University of Colorado, Boulder, CO.

The concept of Coulomb thrusting or Coulomb Formation Flying (CFF) is first introduced by King et al. in Reference 4. CFF uses Coulomb forces to control the distances between spacecraft to achieve the desired relative motion. Spacecraft will naturally charge to either positive or negative voltages due to their interaction with the local space plasma environment. The spacecraft charge level can be actively controlled by continuously emitting electrons or ions as used on the current CLUSTER mission.[5,6] The fuel-efficiency of Coulomb thrusting is at least 3–5 orders greater than that of Electric Propulsion (EP), and typically requires only a few Watts of electrical power to operate.[4] A challenge of CFF is that, unlike conventional thrusters that can produce a thrust vector in any direction, the Coulomb forces only lie along the line-of-sight directions between spacecraft. But this is less of an issue in using Coulomb forces to avoid a collision. The most important factor in preventing collision is the separation distance, which can be fully controlled using Coulomb forces. Another challenge of CFF is that the sparse space plasma will shield electrostatic charges. This effect will reduce the amount of electrostatic force that a neighboring charged spacecraft will experience. The amount of shielding is characterized by the Debye length[7,8] At separation distances greater than a Debye length the perceived inter-craft Coulomb force quickly becomes negligible. At LEO where the plasma is relatively dense and cold, the Debye length is on the order of centimeters. This results in a strong shielding of Coulomb forces and makes Coulomb thrusting un-feasible. However, at GEO the Debye lengths range between 100–1000 meters.[4,9] At 1 AU in deep space the Debye length ranges around 20–50 meters.[4] This makes the Coulomb thrusting concept feasible for HEO and deep space missions while the minimum separation distances are less than 100 meters.

The CFF concept has been investigated for several different mission scenarios. Lappas et al. in Reference 10 develop a hybrid propulsion strategy by combining Coulomb forces and standard electric thrusters for formation flying on the orders of tens of meters in GEO. Reference 11 analyses the stability of a spinning 2-craft Coulomb tether. It shows that if the Debye length is larger than the separation distance, the nonlinear radial motion is locally stable, otherwise unstable. And the perturbed out-of-plane motion is always stable regardless of Debye length. Vasavada and Schaub in Reference 12 present analytical tools to determine the charge solution for a static 4–craft formation. Reference 13 designs a two-stage charge feedback control strategy for a 1–D constrained Coulomb structure. It also analyses the condition for symmetric relative motions of Coulomb structure to be stabilizable by investigating the total energy of the system. Hussein and Schaub derive the collinear three-craft spinning family of solutions in Reference 14. A feedback control based on the linearized model is designed to stabilize a collinear virtual Coulomb tether system. Asymptotic stability is achieved if the system's angular momentum is equivalent to that of the desired equilibrium. However, none of these CFF related works consider the issue of performing active collision avoidance. Such a capability will be required when considering flying larger numbers of craft in close proximity.

Reference 15 is the first publication that develops a collision avoidance strategy using only Coulomb forces. The controller is designed based on Lyapunov stability analysis and requires only feedback on separation distance and distance rate . Without charge saturations the controller can prevent any collision. Considering charge saturations, the paper finds the analytical criteria for an avoidable collision are determined by assuming the Debye length to be infinity. While this feedback control strategy can maintain specified safety separation distances, this control will cause the craft to depart in a different direction from when the collision avoidance maneuver started. This change in direction should be avoided if possible to not re-direct the craft and cause them to approach another craft.

An early version of an patched-conic charged collision avoidance strategy is presented in Reference 16. An open-loop control approach to prevent the collision is presented which aims to maintain the initial velocity vector magnitudes and directions of the approaching craft. By assuming the Debye length to be large compared to the separation distance, and that the spacecraft charges are piece-wise constant, the relative EOM has exactly the same form as Gravitational 2-Body Problem (G2BP). Thus the relative trajectory of the spacecraft is a conic section.[17] Through switching the value of the spacecraft charges, a patched conic section trajectory is investigated which will satisfy the separation distance and the departure velocity requirements. However, this paper does not resolve a duality issue that arises in computing the piece-wise constant charges. Further, no charge optimality or collision avoidance criteria are discussed.

This paper extends the work in Reference 16. The craft are still assumed to be free-flying in deep space

apart from the gravitational attraction of a celestial body. The duality issue in the numerical search routine arising from solving a quadratic equation for the spacecraft charge is fully analyzed. Of interest is determine which of the charge solutions leads to the desired open-loop trajectory. This strategy not only resolves the duality issue, but also manages whether the midpoint of the symmetric trajectory is the periapsis or apoapsis of Phase II. By studying the remaining one DOF of the algorithm proposed in Reference 16, this paper demonstrates the feasibility of optimizing the symmetric collision avoidance trajectory according to a specific cost function. The geometries of the symmetric trajectories are explored to investigate charge optimality of the resulting open-loop maneuvers. This is important when the limited charge capability of actual craft are taken into consideration. Further, given a maximum charging capability, initial condition criteria which lead to a successful collision avoidance maneuver are explored.

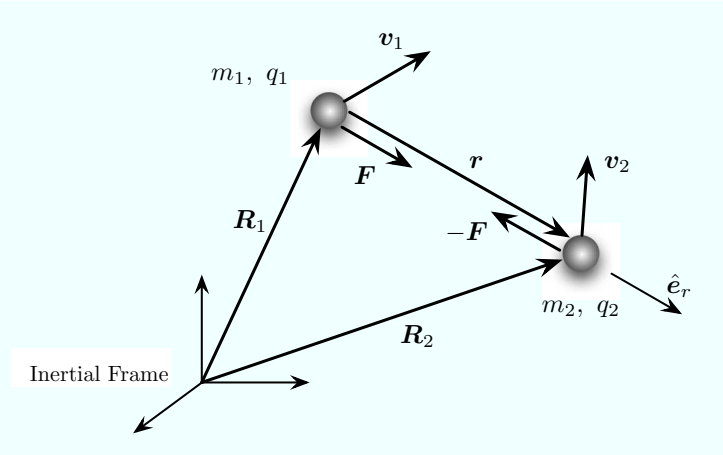

Figure 1. Illustration of the 2-spacecraft system.

CHARGED SPACECRAFT EQUATIONS OF MOTION

This paper considers two spacecraft free-flying in 3-dimensional space where there are no external forces acting on the system. The scenario of the two body system is shown in Figure 1. Assuming point-charge models for the spacecraft, the partially-shielded electrostatic potential generated by the i^{th} spacecraft in a plasma environment is given by[18]

$$V_i(r) = \frac{1}{4\pi\epsilon_0}\frac{q_i}{r}\exp(-r/\lambda_{\text{d}}) \tag{1}$$

where $k_c = 8.99 \times 10^9 \text{C}^{-2} \cdot \text{N} \cdot \text{m}^2$ is the Coulomb constant, and r is the separation distance between the i^{th} spacecraft and the point of interest. The corresponding electrostatic field is obtained by taking the gradient of the potential:

$$E_i(\boldsymbol{r}) = -\nabla_{\boldsymbol{r}} V_i(r) = k_c \frac{q_i}{r^2}\left(1 + \frac{r}{\lambda_{\text{d}}}\right)\exp\left(-\frac{r}{\lambda_{\text{d}}}\right)\hat{\boldsymbol{e}}_r \tag{2}$$

where $\boldsymbol{r}$ is the inertial position vector pointing from the i^{th} spacecraft to the point of interest, $\hat{\boldsymbol{e}}_r$ is the unit vector of $\boldsymbol{r}$. Thus the Coulomb force between the two spacecraft, acting on m_1, is

$$\boldsymbol{F} = q_1 E_2(\boldsymbol{r}_{21}) = k_c \frac{q_1 q_2}{r^2}\left(1 + \frac{r}{\lambda_{\text{d}}}\right)e^{-\frac{r}{\lambda_d}}\hat{\boldsymbol{e}}_{21} = -k_c \frac{q_1 q_2}{r^2}\left(1 + \frac{r}{\lambda_{\text{d}}}\right)e^{-\frac{r}{\lambda_d}}\hat{\boldsymbol{e}}_{12} \tag{3}$$

where $\boldsymbol{r}_{12}$ is the relative position vector from spacecraft 1 (SC1) to spacecraft 2 (SC2), $\hat{\boldsymbol{e}}_{12}$ is the unit vector of $\boldsymbol{r}_{12}$. In the remaining context, we use $\hat{\boldsymbol{e}}_r$ to represent $\hat{\boldsymbol{e}}_{12}$ for brief notation. From the expression of the Coulomb force, it can be seen that the smaller the plasma Debye length is, the shorter the effective range is

of a given electrical charge. For high Earth orbits the Debye length ranges between 100–1000 meters.[4,19,9] CFF typically has spacecraft separation distances less than 100 meters. In deep space at 1 AU distance from the sun the Debye length can vary between 30–50 meters.

The inertial equations of motion of the two charged spacecraft are

$$m_1\ddot{\boldsymbol{R}}_1 = -k_c\frac{q_1q_2}{r^2}\left(1+\frac{r}{\lambda_\mathrm{d}}\right)e^{-\frac{r}{\lambda_\mathrm{d}}}\hat{\boldsymbol{e}}_r \tag{4a}$$

$$m_2\ddot{\boldsymbol{R}}_2 = k_c\frac{q_1q_2}{r^2}\left(1+\frac{r}{\lambda_\mathrm{d}}\right)e^{-\frac{r}{\lambda_\mathrm{d}}}\hat{\boldsymbol{e}}_r \tag{4b}$$

where $\boldsymbol{R}_i$ is the inertial position vector of the i^{th} spacecraft. The inertial relative acceleration vector $\ddot{\boldsymbol{r}}$ is

$$\ddot{\boldsymbol{r}} = \ddot{\boldsymbol{R}}_2 - \ddot{\boldsymbol{R}}_1 = \frac{k_cq_1q_2}{m_1m_2r^2}(m_1+m_2)\left(1+\frac{r}{\lambda_\mathrm{d}}\right)e^{-\frac{r}{\lambda_\mathrm{d}}}\hat{\boldsymbol{e}}_r \tag{5}$$

Note that these equations do not explicitly consider planetary gravity acting on the spacecraft. However, if the collision avoidance maneuver time is very small compared to the cluster orbital period, then they can also be considered an approximation of the charged relative orbital motion. For example, a GEO spacecraft collision avoidance maneuver which takes minutes would be very short compared to the 1 day orbit period, and thus the relative orbital motion would have a secondary effect on the relative motion.

This paper finds a symmetric patched conic section trajectory to prevent a collision, while forcing the departure velocity vector to be the same as the initial arrival velocity vector. Reference 17 shows that if $\lambda_\mathrm{d} \to \infty$, and the charge product $Q = q_1q_2$ is constant, then the relative motion trajectory of the two spacecraft is a conic section. Letting $\lambda_\mathrm{d} \to \infty$ and defining

$$\mu = -k_c\frac{Q(m_1+m_2)}{m_1m_2} \tag{6}$$

Eq. (5) is rewritten as

$$\ddot{\boldsymbol{r}} = -\frac{\mu}{r^3}\boldsymbol{r} \tag{7}$$

Eq. (7) has exactly the same algebraic form as the EOM of G2BP. If the charge product Q is constant, then the effective gravitational coefficient μ is also constant. Thus the resulting motion can be described by a conic section. Note that here μ can be positive or negative. The opposite charge sign case $Q < 0$ results in a positive effective gravitational constant $\mu > 0$. In this case Eq. (7) is exactly the same as the G2BP. If $Q > 0$ and $\mu < 0$, then the relative trajectory is a repulsive hyperbola, where SC2 is moving along a hyperbola, and SC1 stays at the farther focus point.[17]

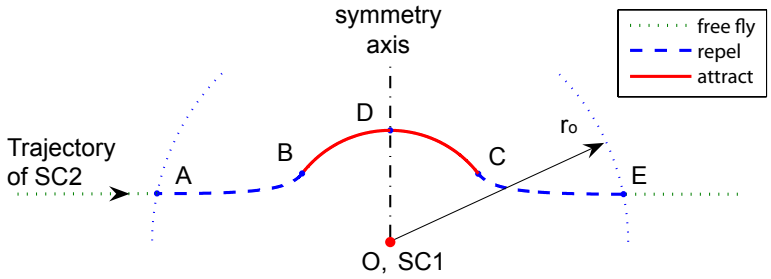

Figure 2 Illustration of the symmetric patched conic section relative motion trajectory with respect to mass m_1.

3-PHASE SYMMETRIC TRAJECTORY SCENARIO

For a two spacecraft system controlled only by Coulomb forces, generally there are an infinity of possible charge and charge switching time solutions which achieve a collision avoidance. This paper investigates a symmetric trajectory programming approach to avoid a collision as well as hold the relative velocity.

An example of the symmetric relative trajectory scenario is shown in Figure 2. The controlled part of the symmetric trajectory is composed of three phases: repel–attract–repel. At the beginning, the two spacecraft are flying freely and approaching each other such that their minimum separation distance will violate a desired safety distance r_s. At the point A, the separation distance r between the spacecraft reaches a potential collision region range r_o. The spacecraft are charged such that $Q > 0$ and the spacecraft start to repel each other to avoid the collision. The magnitude of the charge product is held constant in Phase I until point B is reached. Thus the trajectory $\widehat{AB}$ is a repulsive hyperbola. At point B the charge product switches to a negative value such that the spacecraft are attracting each other. During Phase II from the point B to the point C, the charge product is again held constant. The arc $\widehat{BC}$ is an attractive conic section which can be ellipsis, parabola, or hyperbola depending on the relative arrival velocity magnitude. At the point C the charge product switches back to the same value as in arc $\widehat{AB}$ to produce a symmetric trajectory to $\widehat{AB}$. At the point E, the charges are turned off and the spacecraft begin to fly freely in space. The entire trajectory is symmetric about the axis $\overline{OD}$. The symmetry axis $\overline{OD}$ is the line crossing SC1 and perpendicular to the initial relative velocity.

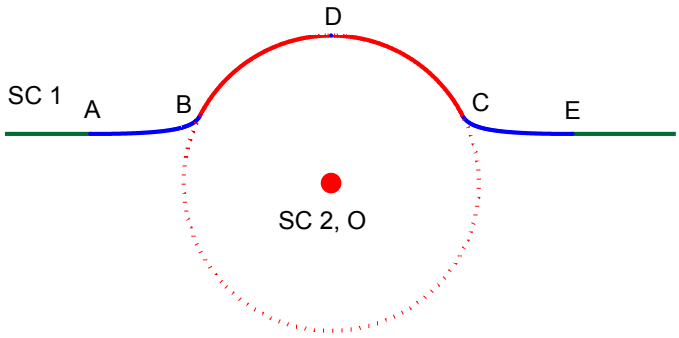

Figure 3. Scenario of the circular Phase II trajectory.

CIRCULAR TRANSITIONAL ORBIT PROGRAMMING

Before studying the general symmetric trajectories, let us at first investigate a special case where the Phase II trajectory is a section of a circle as illustrated in Figure 3. Assume that the relative position vector $\boldsymbol{r}_A$ and the relative velocity $\dot{\boldsymbol{r}}_A$ at point A can be measured. From the description of the symmetric trajectory scenario in the last section there are five unknown parameters that need to be determined: three charge products $Q_{\rm I}$, $Q_{\rm II}$ and $Q_{\rm III}$, and two charge switching times at points B and C. To solve for these five variables some constraints need be clarified.

Constraints

For Phase I $\widehat{AB}$ and Phase III $\widehat{CE}$ to be symmetric, the charge products should be the same value. Thus the first constraint is

$$Q_{\rm III} = Q_{\rm I} \tag{8}$$

Because the trajectory of Phase II $\widehat{BC}$ is a section of a circle, its shape is always symmetric about the symmetry axis $\overline{OD}$. Then a symmetric arc $\widehat{BC}$ requires that the angle $\angle DOC$ satisfies

$$\angle DOC = \angle BOD \tag{9}$$

The point B connects Phase I and Phase II. Thus $\dot{\boldsymbol{r}}_B$ must be perpendicular to $\boldsymbol{r}_B$ because Phase II is circular. This implies the point B is the periapsis of Phase I. This results in the third constraint:

$$r_B = r_{p\mathrm{I}} \tag{10}$$

The trajectory of Phase II is a section of a circle, this requirement can be formulated using the angular momentum magnitude:

$$h_{\mathrm{II}}^2 = \mu_{\mathrm{II}} r_B \tag{11}$$

The collision avoidance task requires that the separation distance $r(t)$ must be greater than a certain safe-restraint distance r_s for all time:

$$r(t) \geq r_s \tag{12}$$

This constraint is global and comes from the collision avoidance mission. For the convenience of calculation, this safety constraint is expressed by the condition

$$r_{\min} = \gamma r_s \tag{13}$$

where $\gamma \geq 1$. In the case that Phase II is a section of a circle, $r_{\min} = r_B$. Thus the final safety constraint for a circular transitional symmetric trajectory is

$$r_B = \gamma r_s \tag{14}$$

Now five constraints in Eqs. (8)–(11), and (14) have been found.

Circular Transitional Orbit Algorithm

The symmetric constraint in Eq. (8) provides Q_{III} once Q_{I} is obtained. Note that the angle $\angle DOC$ is the true anomaly angle (in case the point D is the periapsis) of Phase II. Once the conic section properties of Phase II, which are determined by Q_{II}, are achieved, the charge switching time at the point C is then solved by using Kepler's equation and the symmetry constraint in Eq. (9).

Now there are three variables $(Q_{\mathrm{I}}, Q_{\mathrm{II}}, t_{\mathrm{I}})$ left out of the five unknown parameters that still need to be determined. The conic section properties of Phase I are solved using $\boldsymbol{r}_A$ and $\dot{\boldsymbol{r}}_A$. The eccentricity vector of Phase I is

$$\boldsymbol{c}_{\mathrm{I}} = \dot{\boldsymbol{r}}_A \times \boldsymbol{h} - \frac{\mu_{\mathrm{I}}}{r_A} \boldsymbol{r}_A \tag{15}$$

where $r_A = |\boldsymbol{r}_A|$, $\boldsymbol{h} = \boldsymbol{r}_A \times \dot{\boldsymbol{r}}_A$ is the specific angular momentum of the system, and

$$\mu_{\mathrm{I}} = -k_c \frac{Q_{\mathrm{I}}(m_1 + m_2)}{m_1 m_2} \tag{16}$$

is the effective gravitational coefficient of Phase I. Note that through Eq. (6) finding the charge products Q_{I} and Q_{II} is equivalent to finding μ_{I} and μ_{II}. The vector $\boldsymbol{h}$ is constant by the assumption that there are no external forces acting on the sytem. The eccentricity and semi-major axis of Phase I are calculated by

$$e_{\mathrm{I}} = -\frac{\|\boldsymbol{c}_{\mathrm{I}}\|}{\mu_{\mathrm{I}}} \tag{17a}$$

$$a_{\mathrm{I}} = \frac{r_A \mu_{\mathrm{I}}}{2\mu_{\mathrm{I}} - r_A v_A^2} \tag{17b}$$

where $v_A = \|\dot{\boldsymbol{r}}_A\|$ is the magnitude of the relative velocity vector. The angle $\angle AOD$ is calculated as

$$\angle AOD = \arctan\left(\frac{h}{r_A v_A}\right) - \frac{\pi}{2} \tag{18}$$

Utilizing the constraint that the point B must be the periapsis of Phase I, the charge switching time t_B at point B is calculated through

$$t_B = \frac{|N_{AI}|}{\sqrt{\mu_I/a_I}} \tag{19}$$

with the right hand side of this equation being completely determined by μ_I, which in return is determined by Q_I. Thus, it can be concluded that the Phase I trajectory are determined by the charge product Q_I.

The radius r_B is calculated by

$$r_B = \frac{h^2/\mu_I}{1-e_I} \tag{20}$$

where the eccentricity e_I is given by Eq. (17a). Substituting Eq. (20) into the safety constraint in Eq. (14) and multiplying both sides by $\mu_I(1-e_I)/(\gamma r_s)$, yield

$$\mu_I(1-e_I) = \frac{h^2}{\gamma r_s} \tag{21}$$

Subtracting both sides by μ_I, taking square of both sides and using $e_I = -\frac{\|\boldsymbol{c}\|}{\mu_I} = \|\frac{\boldsymbol{r}_A}{r_A} - \frac{\dot{\boldsymbol{r}}_A \times \boldsymbol{h}}{\mu_I}\|$, yield

$$\mu_I^2 e_I^2 = \mu_I^2 - 2\mu_I \dot{\boldsymbol{r}}_A \times \boldsymbol{h} \cdot \boldsymbol{r}_A / r_A + \dot{\boldsymbol{r}}_A \times \boldsymbol{h} \cdot \dot{\boldsymbol{r}}_A \times \boldsymbol{h} \tag{22}$$

Substituting Eq. (22) into Eq. (21), yields

$$-2\mu_I \dot{\boldsymbol{r}}_A \times \boldsymbol{h} \cdot \boldsymbol{r}_A / r_A + \dot{\boldsymbol{r}}_A \times \boldsymbol{h} \cdot \dot{\boldsymbol{r}}_A \times \boldsymbol{h} = \frac{h^4}{\gamma^2 r_s^2} - \frac{2\mu_I h^2}{\gamma r_s} \tag{23}$$

Thus the Phase I effective gravitational coefficient for a circular transitional trajectory is solved by grouping terms containing μ_I:

$$\mu_{I,c} = \frac{1}{2} \frac{\frac{h^4}{\gamma^2 r_s^2} - \dot{\boldsymbol{r}}_A \times \boldsymbol{h} \cdot \dot{\boldsymbol{r}}_A \times \boldsymbol{h}}{\frac{h^2}{\gamma r_s} - \dot{\boldsymbol{r}}_A \times \boldsymbol{h} \cdot \frac{\boldsymbol{r}_A}{r_A}} \tag{24}$$

After obtaining $\mu_{I,c}$, the variable t_I is determined by Eq. (19). These values of μ_I and t_I ensure that at the point B the relative speed vector is perpendicular to the relative position vector, meanwhile the safety constraint $r_B = \gamma r_s$ is also satisfied.

The next step is to find a proper Q_{II} or μ_{II} that results in a circular orbit. Using the constraint for a circular transitional orbit in Eq. (11), μ_{II} is found to be

$$\mu_{II,c} = \frac{h^2}{r_B} = \frac{h^2}{\gamma r_s} \tag{25}$$

To find the Phase II duration time t_{II}, the Phase II symmetry constraint in Eq. (9) is utilized. Note that the angular velocity is constant in Phase II, the duration time is proportional to the angle $\angle BOC$ as:

$$t_{II,c} = \angle BOC \cdot \frac{T_{II}}{2\pi} = 2\angle BOD \cdot \frac{T_{II}}{2\pi} = \frac{\angle BOD \cdot T_{II}}{\pi} \tag{26}$$

where the period of the Phase II circular orbit is $T_{II} = \sqrt{\mu_{II}/r_{II}^3}$, the angle $\angle BOD$ is given by

$$\angle BOD = \angle AOD - |f_{AI}| = \angle AOD + \text{atan}\left(\frac{\hat{\boldsymbol{i}}_{cI} \times \hat{\boldsymbol{i}}_{rA} \cdot \hat{\boldsymbol{i}}_h}{\hat{\boldsymbol{i}}_{cI} \cdot \hat{\boldsymbol{i}}_{rA}}\right) \tag{27}$$

where $\hat{\boldsymbol{i}}_{cI}$, $\hat{\boldsymbol{i}}_{rA}$ and $\hat{\boldsymbol{i}}_h$ are the unit vectors of $\boldsymbol{c}_I$, $\boldsymbol{r}_A$ and $\boldsymbol{h}$ respectively. The angle $\angle AOD$ is expressed in Eq. (18).

Thus a symmetric trajectory with Phase II being a part of a circular orbit has been found. Specifically, the variables μ_I, μ_{II}, Q_{III}, t_B, t_{II} are calculated through Eqs. (24), (25), (8), (19) and (26), respectively. Note that this circular transitional trajectory solution is calculated analytically.

GENERAL SYMMETRIC TRAJECTORY PROGRAMMING STRATEGY

After solving a circular Phase II trajectory in the last section, this section investigates the more general symmetric collision avoidance trajectory with the Phase II trajectory being any type of conic section.

A general 3-Phase symmetric trajectory is shown in Figure 2. As mentioned in the last section, as with the circular Phase II case, there are five unknowns that need to be determined: $[Q_{\rm I}, Q_{\rm II}, Q_{\rm III}, t_B, t_{\rm II}]$.

Constraints

The general constraints are largely the same as those for the circular transitional orbit. The three constraints in Eqs. (8), (9), and (13) are directly used to find a general symmetric trajectory. Because here the Phase II trajectory is a part of general conic section, the circular constraints in Eqs. (10) and (11) are not applicable.

Since the arc $\widehat{BC}$ is not a part of a circle, for Phase II to be symmetric about the axis $\overline{OD}$, the point D must be the periapsis or apoapsis of Phase II, unless the arc $\widehat{BC}$ is a part of a circular orbit. This requirement is formulated as:

$$r_D = r_{p,\rm II}, \quad \text{or} \quad r_D = r_{a,\rm II} \tag{28}$$

where $r_{p,\rm II}$ and $r_{a,\rm II}$ are the periapsis radius and the apoapsis radius of Phase II.

Now there are four equality constraints to solve the patched conic collision avoidance trajectory. Eqs. (8), (9) and (28) are from the symmetric patched conic section properties. These three constraints ensure a symmetric trajectory. The constraint given by Eq. (14) is required by the collision avoidance task. To complete the 5-variable searching problem, one more constraint is needed.

Note that the four equality constraints ensure a collision avoidance and meanwhile result in a symmetric trajectory, which means the symmetric trajectory programming requirements have been satisfied. The remaining one degree of freedom actually provides a flexibility in solving for the five variables. Here this section assumes a proper value of $Q_{\rm I}$, then constructs a closed-loop numerical iteration routine to find other four variables. This iteration routine can be used as a part of the charge-optimal trajectory programming problem which updates $Q_{\rm I}$ such that a certain charge cost function is minimized. The charge-optimization examples are shown and discussed in the numerical simulation section.

General Numerical Iteration Routine

Assuming that a proper value of $Q_{\rm I}$ has been given, this section develops a numerical iteration routine to find a symmetric patched conic section trajectory to avoid a potential collision. The charge product $Q_{\rm I}$ and the initial conditions $[\boldsymbol{r}_A, \dot{\boldsymbol{r}}_A]$ determine the conic section of Phase I. Without loss of generality, assume that $t_A = 0$. If t_B is given, the angle $\angle AOB$ can be calculated using Kepler's equation in Phase I. The states $[\boldsymbol{r}_B, \dot{\boldsymbol{r}}_B]$ are also determined by solving the orbit EOM of Phase I. Utilizing the constraint that the point D must be the periapsis or apoapsis of Phase II, the point C is determined by the constraint in Eq. (9). Phase III is determined by the state of point C, which can be infered from t_B. Thus the charge switching time variable t_B logically determines the whole patched conic section trajectory. In the numerical iteration routine, t_B is chosen as the variable to be propagated.

Because t_B has been chosen as the variable to be propagated in the iteration loop, it starts from an initial guess value, and is updated using an error of a target function. In the present formulation of the algorithm the time point t_B is assumed to be given. The states at point B are determined by using the conic section properties of Phase I. The mean hyperbolic anomaly of point B considered in Phase I is calculated using the Kepler's equation:

$$N_{B\rm I} = N_{A\rm I} + \sqrt{\frac{\mu_{\rm I}}{a_{\rm I}^3}} \cdot t_B = N_{A\rm I} + n_{\rm I} \cdot t_B \tag{29}$$

Then the hyperbolic anomaly $H_{B\rm I}$ is calculated by numerically solving the standard anomaly relationship:[20]

$$N_{B\rm I} = e_{\rm I}\sinh(H_{B\rm I}) + H_{B\rm I} \tag{30}$$

Thus the true anomaly of point B in Phase I is determined by

$$f_{B,\mathrm{I}} = 2 \cdot \arctan\left(\tanh\left(\frac{H_{B\mathrm{I}}}{2}\right)\sqrt{\frac{e_{\mathrm{I}}+1}{e_{\mathrm{I}}-1}}\right) \tag{31}$$

The radius and the magnitude of the relative velocity at point B are

$$r_B = \frac{h^2/\mu_{\mathrm{I}}}{1 - e_{\mathrm{I}}\cos f_{B\mathrm{I}}} \tag{32a}$$

$$v_B = \sqrt{\mu_{\mathrm{I}}\left(\frac{2}{r_B} - \frac{1}{a_{\mathrm{I}}}\right)} \tag{32b}$$

here h is the magnitude of the specific angular momentum determined by the initial conditions. Eq. (32b) is obtained from the energy equation.

After obtaining the relative motion states at point B, Phase II is determined by the symmetric conic section constraints. Specifically, the charge product Q_{II} and point C are determined through the following process. At first, the angle $\angle AOB$ is calculated by

$$\angle AOB = |f_{B,\mathrm{I}} - f_{A,\mathrm{I}}| \tag{33}$$

The angle $\angle BOD$ is determined by the geometry relation:

$$\angle BOD = \angle AOD - \angle AOB \tag{34}$$

According to the symmetric constraint in Eq. (9), the angle

$$\angle COD = \angle BOD \tag{35}$$

is determined. Thus the point C is located. Note that of the five variables which determine the symmetric conic section trajectory, the points B, C, the charge products Q_{I}, Q_{III} have been solved. The only variable left to be determined is the charge product Q_{II}. Solving for μ from Eq. (7) yields

$$\mu_{\mathrm{II}} = -k_c\frac{Q_{\mathrm{II}}(m_1+m_2)}{m_1 m_2} \tag{36}$$

Once μ_{II} is solved, Q_{II} is also determined. The following development solves for μ_{II} based on the states of the point B and the symmetric constraints.

Since the arc $\widehat{BC}$ is a part of a conic section, it has all of the properties of conic section orbit. Utilizing the vis-viva equation, the eccentricity e is expressed as:

$$e = \sqrt{1 + \left(\frac{v^2}{\mu} - \frac{2}{r}\right)\frac{h^2}{\mu}} \tag{37}$$

Because h is constant by the assumption that no external forces act on the system, the expression of the eccentricity in Eq. (37) contains only three unknown variables r, v and μ. Substituting Eq. (37) into the radius equation, yields

$$r = \frac{h^2}{\mu + \cos f\sqrt{\mu^2 + \left(v^2 - \frac{2\mu}{r}\right)h^2}} \tag{38}$$

Transforming Eq. (38) to separate the square root term, yields

$$\cos f\sqrt{\mu^2 + \left(v^2 - \frac{2\mu}{r}\right)h^2} = \frac{h^2}{r} - \mu \tag{39}$$

Squaring Eq. (39) and using the fact that $1-\cos^2 f = \sin^2 f$, Eq. (39) is simplified to be

$$\sin^2 f\,\mu^2 - \frac{2h^2}{r}\sin^2 f\,\mu - \cos^2 f\,v^2h^2 + \frac{h^4}{r^2} = 0 \tag{40}$$

With h being constant, this equation contains four variables μ, f, r and v. Note that Eq. (40) is valid for all conic section orbits. Evaluating f, r and v at point B in Phase II, Eq. (40) becomes a quadratic equation of μ. r_B and v_B are given by Eq. (32). By the symmetry constraint, the point D can only be the periapsis or apoapsis of Phase II. If the point D is the periapsis, then

$$f_{B,\mathrm{II}} = -\angle BOD \tag{41}$$

Otherwise D is the apoapsis of Phase II with

$$f_{B,\mathrm{II}} = \pi - \angle BOD \tag{42}$$

In both cases, the resulting final equations after substituting $f_{B\mathrm{II}}$ into Eq. (40) are identical:

$$\underbrace{\sin^2\angle BOD}_{l_1}\,\mu_{\mathrm{II}}^2 \underbrace{-\frac{2h^2}{r_B}\sin^2\angle BOD}_{l_2}\,\mu_{\mathrm{II}} \underbrace{-\cos^2\angle BOD\,v_B^2h^2 + \frac{h^4}{r_B^2}}_{l3} = 0 \tag{43}$$

Analytically solving for μ_{II} from Eq. (43), the charge product in Phase II is then obtained by Eq. (36).

Note that given μ_{I}, t_B and $\angle BOD$, generally there are two solutions of μ_{II} to Eq. (43). The solutions are

$$\mu_{\mathrm{II}}^{(1)} = \frac{h^2}{r_B} + \frac{1}{2\sin^2\angle BOD}\sqrt{l_2^2 - 4l_1l_3} \tag{44a}$$

$$\mu_{\mathrm{II}}^{(2)} = \frac{h^2}{r_B} - \frac{1}{2\sin^2\angle BOD}\sqrt{l_2^2 - 4l_1l_3} \tag{44b}$$

Substituting Eq. (44) into the RHS of Eq. (39), yields

$$\frac{h^2}{r} - \mu = \mp\frac{1}{2\sin^2\angle BOD}\sqrt{l_2^2 - 4l_1l_3} \tag{45}$$

This indicates that the two solutions result in two opposite signs in the RHS of Eq. (39). But for a particular value of f, either $-\angle BOD$ or $\pi - \angle BOD$, the LHS of Eq. (39) only has a specific sign. This means only one of the two solutions to Eq. (43) satisfies Eq. (39). In other words, only one of the two values in Eq. (44) results in a symmetric trajectory.

The plots in Figure 4 show the two scenarios using $\mu_{\mathrm{II}}^{(1,2)}$ given by Eq. (44). Figure 4(a) shows the case that the point D is expected to be the periapsis of Phase II. Figure 4(b) shows the case that the point D is designated as the apoapsis of Phase II. In Figure 4(a), the angle $\angle BOD = 71.9°$, and $f_{B,\mathrm{II}}$ is expected to be $-\angle BOD = -71.9°$. With this value of $f_{B,\mathrm{II}}$, the LHS of Eq. (39) must be positive. Correspondingly, only $\mu_{\mathrm{II}}^{(2)}$ satisfies Eq. (39). This is confirmed by Figure 4(a). Figure 4(b) confirms the other case that only $\mu_{\mathrm{II}}^{(1)}$ results in the symmetric trajectory with the point D being the apoapsis of Phase II.

By assuming that the variables Q_{I} and t_B are given, the previous development outlines how to solve for the states at the points B and C, and the charge product of Phase II Q_{II}. However, in our present collision avoidance application t_B is not explicity determined and will need to be solved using a numerical search routine. Note that three constraints have been used in deriving these formulas, Eqs. (8), (28), and (9). Next the safety constraint in Eq. (13) needs to be utilized. The numerical search routine is intended to find an appropriate t_B such that the closest distance $r_{\min} = \gamma r_s$, where $\gamma \geq 1$.

The following theorem provides a rule to find the minimum distance $r_{\min}$ in the whole trajectory.

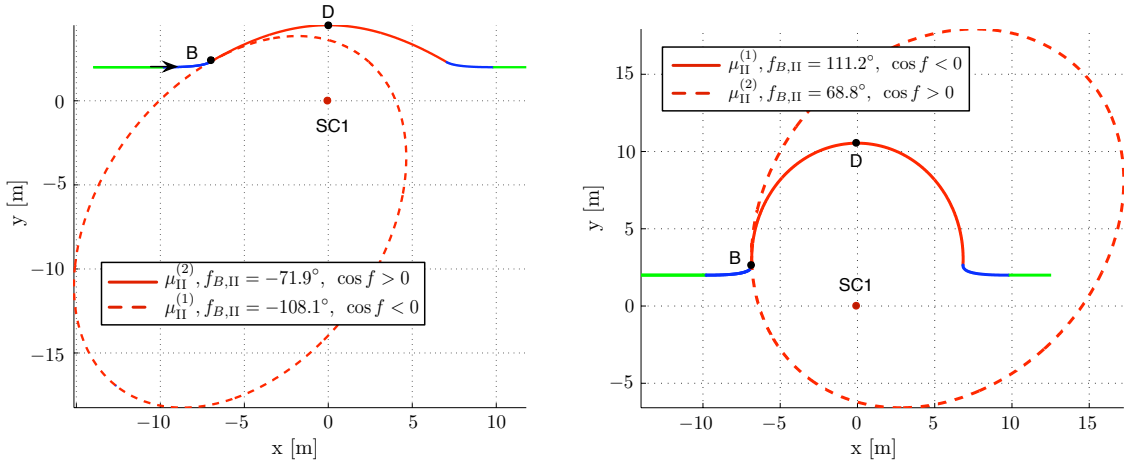

(a) Point D is the periapsis of Phase II.

(b) Point D is the apoapsis of Phase II.

Figure 4 Two cases of using $\mu_{\rm II}^{(1,2)}$ solutions, in both cases only one of the two solutions results in an actual symmetric trajectory.

Theorem 1 *Consider the 3-Phase symmetric patched conic section trajectory as shown by Figure 2. If the point D is the periapsis of Phase II, then the minimum distance of the entire $\widehat{AE}$ trajectory is the periapsis radius of Phase II, i.e.:*

$$r_{min} = r_{p,II} \tag{46}$$

If the point D is the apoapsis of Phase II, then the minimum distance is the periapsis radius of Phase I, i.e.:

$$r_{min} = r_{p,I} \tag{47}$$

Proof If D is the periapsis of Phase II, then $r_{p,\rm II}$ is the minimum distance in Phase II. So it's true that $r_{p,\rm II} < r_B$. Because $\angle BOD < 90°$, $f_{B,\rm II} \in (-90, 0)°$, thus $\dot{r}_B < 0$. Then the periapsis of Phase I does not lie along the arc $\widehat{AB}$. This indicates that throughout Phase I $\dot{r} < 0$. Thus r_B is the minimum distance in Phase I. Because $r_{p,\rm II} < r_B$, $r_{p,\rm II}$ is the minimum distance in the entire trajectory.

If D is the apoapsis of Phase II, then r_B is the minimum distance in Phase II because $f_{B,\rm II} \in (90, 180)°$and $\dot{r}_B > 0$. Note that if $\dot{r}_A < 0$, then the periapsis of Phase I must lie in the arc $\widehat{AB}$ because $\dot{r}$ crosses zero in Phase I. So $r_{p,\rm I}$ is the minimum distance in Phase I, this indicates that $r_{p,\rm I} < r_B$. Because r_B is the minimum distance in Phase II, $r_{p,\rm I}$ is the minimum distance in the entire trajectory. □

Theorem 1 states that if point D is the periapsis of Phase II, then the periapsis of Phase I must not lie on the arc $\widehat{AB}$. If point D is the apoapsis of Phase II, then the periapsis of Phase I must lie on the arc $\widehat{AB}$. Because the periapsis of Phase I lies in $\widehat{AB}$, $\dot{r}$ must cross zero in Phase I. Figure 5(b) illustrates this scenario in detail.

Figure 6 shows the change of $r_{p,\rm II}$ w.r.t. t_B assuming that $\mu_{\rm I}$ is held fixed. The variable $t_{p,\rm I}$ is the time for SC2 to fly from the point A to the periapsis of Phase I. It can be seen that when $t_B < t_{p,\rm I}$ and $\mu_{\rm II}^{(2)}$ is used, $r_{p,\rm II}$ is monotonically increasing as t_B increases; when $t_B > t_{p,\rm I}$ and $\mu_{\rm II}^{(1)}$ is used, $r_{p,\rm II}$ is monotonically decreasing as t_B increases. Thus a symmetric collision avoidance trajectory with the point D being the periapsis of Phase II can be found by initializing $t_B^{(0)} < t_{p,\rm I}$ and updating t_B using a common numerical methods such as Newton's method or the Secant method.

Alternatively initializing $t_B^{(0)} > t_{p,\rm I}$ and using $\mu_{\rm II}^{(1)}$ lead to a symmetric collision avoidance trajectory with the point D being the apoapsis of Phase II. Note that this solution yields $r_{p,\rm II} = \gamma r_s$ which is a conservative

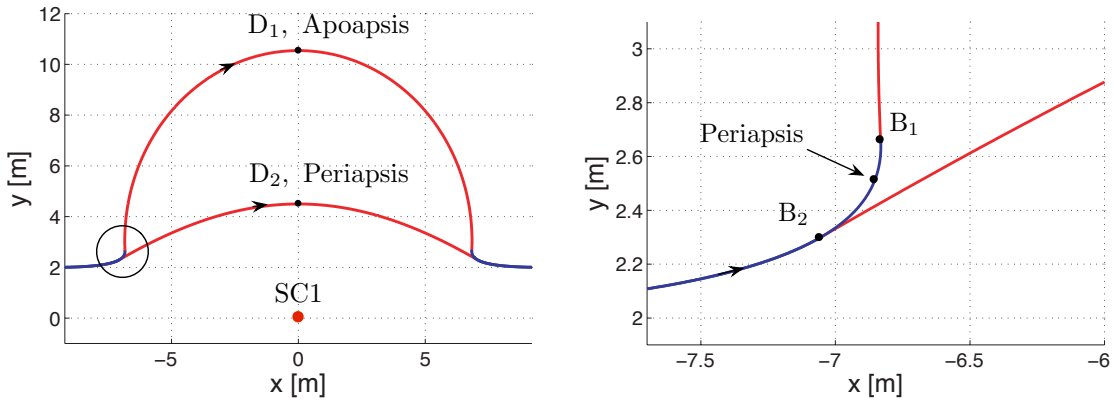

(a) Big scenario.

(b) Focused on Phase I–Phase II connecting points.

Figure 5. Illustration of the two cases with the point D being the periapsis and apoapsis of Phase II.

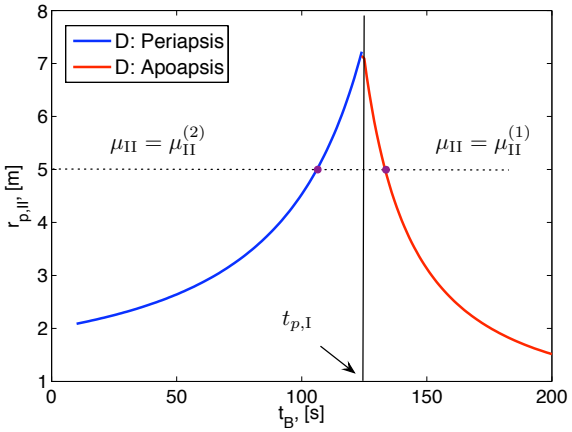

Figure 6. Given μ_{I}, the resulting $r_{p,\mathrm{II}}$ w.r.t. t_B.

maneuver because the point D is the apoapsis of Phase II. Another way to achieve the solution with the point D being the apoapsis is to set $r_{p,\mathrm{I}} = \gamma r_s$, and solve for corresponding μ_{I} from Eq. (24). Any symmetric trajectory with the point D being the apoapsis of Phase II will satisfy collision avoidance requirement. Thus there are infinite choices of t_B which lead to symmetric maneuvers and varying apoapses.

Before performing a numerical search for t_B for a given μ_{I} it must be decided apriori whether a periapsis or apoapsis D point solution is being sought. During the numerical iterations the current estimates of t_B must be constrained to remain either larger or smaller than the periapsis time $t_{p,\mathrm{I}}$ of Phase I. If t_B crosses $t_{p,\mathrm{I}}$ without switching the μ_{II} solution, the algorithm will lead to an asymmetric trajectory with $f_{B,\mathrm{II}}$ lying in a wrong quadrant, as shown by the dashed lines in Figure 4.

Note that the path with the point D being the apoapsis of Phase II is a longer path, both in length and in time. Practically speaking, there is a bigger chance for the longer path to be influenced by disturbances. Though in developing the algorithm the Debye length effect is not taken into consideration, this effect does exist in the space environment. Since the longer path will be influenced more due to disturbance, the shorter path with the point D being the periapsis is preferred.

Finally all the required sub-steps have been presented to outline the overall collision avoidance algorithm. The basic logic is to search for a proper t_B^* such that the collision avoidance criteria

$$r_{p,\mathrm{II}} = \gamma r_s \tag{48}$$

is satisfied, with the point D being the periapsis of Phase II. If for some reason t_B^* is not achievable, for example if t_B^* is so short that the spacecraft have missed it already at time t_B^*, the numerical routine switches to find a circular transitional trajectory.

In this paper, Newton's method is used in the numerical searching for t_B^* such that the following target function becomes zero:

$$g(t_B) = r_{p,\mathrm{II}}(t_B) - \gamma r_s \tag{49}$$

The iteration routine to determine a symmetric collision avoidance with D being the periapses of Phase II propagates according to the following steps:

Step 1 *Initialization:* From the measurements $\boldsymbol{r}_A$ and $\dot{\boldsymbol{r}}_A$, calculate e_{I}, a_{I} through Eq. (17), and calculate the angle $\angle AOD$ through Eq. (18). Prescribe a proper μ_{I}, which means $|\mu_{\mathrm{I}}|$ must be greater than $|\mu_{\mathrm{I,c}}|$ to ensure $r_{p,\mathrm{I}} > \gamma r_s$. It must also make sure Q_{I} is implementable, which means $Q_{\mathrm{I}} < Q_{\max}$. Calculate $t_{p,\mathrm{I}}$. Initialize t_B:

$$t_B^{(0)} = \alpha t_{p,\mathrm{I}} \tag{50}$$

where $0 < \alpha < 1$.

Step 2 Solve for the point B's states r_B and v_B through Eqs. (29)–(32).

Step 3 Solve for $\mu_{\mathrm{II}}^{(2)}$ by Eq. (44), using the minus sign. Calculate $r_{p,\mathrm{II}}$ through

$$r_{p,\mathrm{II}} = a_{\mathrm{II}}(1 - e_{\mathrm{II}}) \tag{51}$$

and a_{II} is solved by the energy equation, e_{II} is calculated through Eq. (37) evaluating at point B in Phase II.

Step 4 Calculate $g(t_B)$ by Eq. (49). Judge whether $|g(t_B)| <$ Tol. If yes, **STOP**. Otherwise, go to **Step 5**.

Step 5 Calculate $g' = \frac{\partial g}{\partial t_B}$ using the finite difference method.

Step 6 Update $t_B^{(i+1)} = t_B^{(i)} - \frac{g}{g'}$, $i = i + 1$. Go to **Step 2**.

After choosing a proper value of Q_{I}, this routine calculates a symmetric collision avoidance trajectory composed of three patched conic-sections.

COLLISION AVOIDANCE CRITERIA WITH CHARGE SATURATION

The previous section develops a numerical routine to find a symmetric patched conic section trajectory to avoid the collision and meanwhile preserve the relative velocity magnitude and direction of the two-spacecraft system. In deriving this routine, it is assumed that the charge product of the two spacecraft is unlimited. If the charge product limitation is taken into consideration, the system's ability to avoid a potential collision is then limited. Under certain conditions, for example the two spacecraft are approaching each other too quickly, the collision would be unpreventable. This section determines the criteria to predict whether a potential collision can be prevented using the presented collision avoidance routines.

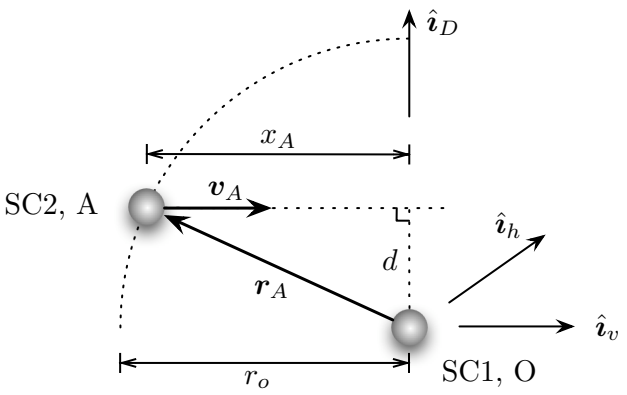

Figure 7. Geometry of the 2-spacecraft system.

Figure 7 illustrates the geometry of the two spacecraft system when the collision avoidance strategy is triggered at time t_A. The vectors $\boldsymbol{r}_A$, $\boldsymbol{v}_A$ and $\boldsymbol{h}$ can be expressed in the $\{\hat{\boldsymbol{i}}_v, \hat{\boldsymbol{i}}_h, \hat{\boldsymbol{i}}_D\}$ * frame as

$$\boldsymbol{r}_A = -x_A \hat{\boldsymbol{i}}_v + d\hat{\boldsymbol{i}}_D \tag{52a}$$

$$\boldsymbol{v}_A = v_0 \hat{\boldsymbol{i}}_v \tag{52b}$$

$$\boldsymbol{h} = \boldsymbol{r}_A \times \boldsymbol{v}_A = dv_0 \hat{\boldsymbol{i}}_h \tag{52c}$$

This section is investigating the critical state with $\gamma = 1$. Substituting Eq. (52) into Eq. (24) and using the fact $\|\boldsymbol{r}_A\| = r_o$, yield

$$\mu_{\text{I,c}} = \frac{r_o\, v_0^2\, d^2 - r_s^2\, r_o\, v_0^2}{2r_s(r_o - r_s)} \tag{53}$$

Eq. (53) privides the value of μ_{I} that results in $r_{p,\text{I}} = r_s$. Thus the circular transitional orbit solution gives μ_{I} in the critical state.

Theorem 2 *Consider a repulsive hyperbola motion governed by Eq.* (7)*, with $\mu < 0$ being constant. Given initial position and velocity $[\boldsymbol{r}_0, \dot{\boldsymbol{r}}_0]$, the radius of the periapsis r_p increases as $|\mu|$ increases.*

Proof To mathematically prove this theorem, it's required to express r_p in terms of μ and initial conditions. For a repulsive hyperbola, the periapsis radius is given as[17]

$$r_p = a(1 + e) \tag{54}$$

Here a and e are actually determined by the initial conditions and μ. Substituting $e = \sqrt{1 - h^2/\mu a}$ and Eq. (17b) into Eq. (54) and using $|\mu| = -\mu$ instead of μ, yield

$$r_p = \frac{1}{2|\mu|/r_0 + v_0^2} \left(|\mu| + \sqrt{|\mu|^2 + h^2\,(2|\mu|/r_0 + v_0^2)} \right) \tag{55}$$

where $r_0 = \|\boldsymbol{r}_0\|$, $v_0 = \|\dot{\boldsymbol{r}}_0\|$, $h = \|\boldsymbol{r}_0 \times \dot{\boldsymbol{r}}_0\|$, which are all determined by the initial conditions.

*$\{\hat{\boldsymbol{i}}_v, \hat{\boldsymbol{i}}_h, \hat{\boldsymbol{i}}_D\}$ centers at SC1, with $\hat{\boldsymbol{i}}_v$ pointing to the SC2's relative velocity direction, $\hat{\boldsymbol{i}}_h$ is the unit vector of the relative angular momentum, $\hat{\boldsymbol{i}}_D$ closes the right hand coordinate.

It's still not obvious to see the trend of r_p as $|\mu|$ increases. Taking a partial derivative of r_p with respect to $|\mu|$, yields

$$\frac{\partial r_p}{\partial |\mu|} = \frac{1 + \left(|\mu| + h^2/r_0\right)/\beta}{2|\mu|/r_0 + v_0^2} - \frac{|\mu| + \beta}{r_0(2|\mu|/r_0 + v_0^2)^2} \tag{56}$$

where $\beta = \sqrt{|\mu|^2 + h^2\left(2|\mu|/r_0 + v_0^2\right)}$. The trend of r_p as μ increases is determined by the sign of $\frac{\partial r_p}{\partial |\mu|}$. Eq. (56) can be changed to be:

$$\frac{\partial r_p}{\partial |\mu|} = \frac{1}{(2|\mu|/r_0 + v_0^2)^2}\left\{ \frac{|\mu|}{r_0} + v_0^2 + \left(\frac{|\mu|^2}{r_0} + |\mu| v_0^2 \right) \Big/ \beta \right\} \tag{57}$$

Eq. (57) gives a simplified expression of $\frac{\partial r_p}{\partial |\mu|}$ with every individual term being positive. Thus the partial derivative $\frac{\partial r_p}{\partial |\mu|}$ is alway positive. This proves that r_p increases as $|\mu|$ increases. □

Applying Theorem 2 in the 3-Phase symmetric patched conic section scenario, yields the following lemma.

Lemma 1 *For the 3-Phase patched conic section scenario as shown in Figure 2, the circular transitional trajectory solution provides the minimum value of Q_I that satisfies the collision avoidance constraint $r_{min} \geq r_s$.*

Proof For the critical case where $\gamma = 1$, the circular transitional trajectory has the following properties:

$$r_{p,\mathrm{I}} = r_s, \qquad r_{\mathrm{II}} = r_s \tag{58}$$

where r_{II} is the radius of Phase II which is constant.

By Theorem 2, $\mu_{\mathrm{I,c}}$ in Eq. (53) provides the minimum value of $|\mu_{\mathrm{I}}|$ that satisfies $r_{p,\mathrm{I}} \geq r_s$. From Eq. (6), the charge product Q_{I} is proportional to $|\mu_{\mathrm{I}}|$, thus the circular transitional trajectory provides the minimum value of Q_{I} such that $r_{p,\mathrm{I}} \geq r_s$. For Phase II, the radius is equal to r_s, which satisfies the collision avoidance requirement. So the circular transitional trajectory solution provides the minimum Q_{I} to avoid the collision. □

Theorem 3 *For the two effective gravitational coefficients given by Eq.* (24) *and Eq.* (25)*, $\mu_{I,c} > |\mu_{II,c}|$ if and only if $d < d^* = r_s\sqrt{\frac{r_o}{3r_o - 2r_s}}$.*

Proof First let us investigate $\mu_{\mathrm{II,c}} - |\mu_{\mathrm{I,c}}|$:

$$\begin{aligned}
\mu_{\mathrm{II,c}} - |\mu_{\mathrm{I,c}}| =& \mu_{\mathrm{II,c}} + \mu_{\mathrm{I,c}} \\
=& \frac{h^2}{r_s} + \frac{r_o v_0^2 d^2 - r_s^2 r_o v_0^2}{2r_s(r_o - r_s)} \\
=& \frac{v_0^2}{2r_s(r_o - r_s)}\Big((3r_o - 2r_s)d^2 - r_o r_s^2\Big)
\end{aligned} \tag{59}$$

When $|\mu_{\mathrm{I,c}}| > \mu_{\mathrm{II,c}}$, $\mu_{\mathrm{II,c}} - |\mu_{\mathrm{I,c}}| < 0$, applying this to the formula in Eq. (59), yields

$$\frac{v_0^2}{2r_s(r_o - r_s)}\Big((3r_o - 2r_s)d^2 - r_o r_s^2\Big) < 0 \quad \Leftrightarrow \quad d < \sqrt{\frac{r_o r_s^2}{3r_o - 2r_s}} = d^* \tag{60}$$

□

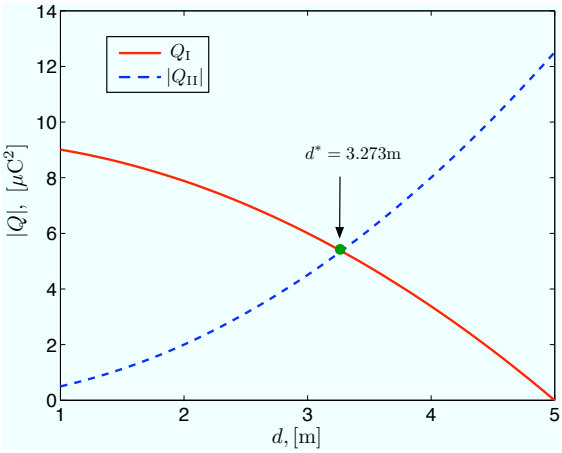

(a) Circular transitional trajectory.

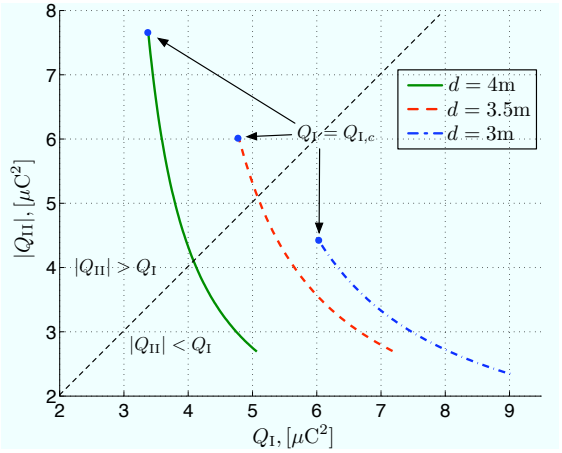

(b) General symmetric trajectory solution, $Q_{\rm I}$–$Q_{\rm II}$ plane.

Figure 8. Charge product values under different d.

Theorem 2 and Lemma 1 show $Q_{\rm I}$ is lower bounded by the circular Phase II solution:

$$Q_{\rm I} \geq Q_{\rm I,c} = -\frac{\mu_{\rm I,c} m_1 m_2}{k_c(m_1+m_2)} = -\frac{(r_o v_0^2 d^2 - r_s^2 r_o v_0^2) m_1 m_2}{2k_c r_s (r_o - r_s)(m_1+m_2)} \tag{61}$$

When implementing these charge collision avoidance solutions, the averaged charge is less of a concern because the spacecraft charge can be servoed with very little electrical power and using essentially no fuel.[4] Instead, the required absolute levels should be made as small as possible. This results in smaller required spacecraft potentials and less issues with electrostatic discharges. Assuming that d satisfies the condition in Theorem 3, then note that the circular transfer orbit provides the minimum $Q_{\rm I}$ collision avoidance solution. To illustrate this, consider the following numerical simulation results with the initial conditions:

$$\boldsymbol{R}_1(t_0) = [0,0,0]^T\text{m},\ \dot{\boldsymbol{R}}_1(t_0) = [0,0,0]^T\text{m/s},\ \boldsymbol{R}_2(t_0) = [20,d,0]^T\text{m},\ \dot{\boldsymbol{R}}_2(t_0) = [-0.03,0,0]^T\text{m/s} \tag{62}$$

and with $r_o = 15$m, $r_s = 5$m. Figure 8 shows the charge product values under different values of the offset distance d. For the circular transitional trajectory case Theorem 3 states that $Q_{\rm I} > Q_{\rm II}$ when $d < 3.2733$m, and this is reflected in Figure 8(a).

For general symmetric trajectory cases, given a value of d, there remains one degree of freedom to determine the collision avoidance trajectory. The numerical algorithm presented in the last section chooses a value of $Q_{\rm I}$ and calculates all the remaining variables. Figure 8(b) shows the value of $|Q_{\rm II}|$ corresponding to $Q_{\rm I}$ under different d, with all other variables the same as in Figure 8(a). The shaded area is the region where $|Q_{\rm II}| > Q_{\rm I}$.

Figure 8(b) illustrates that the solution with $|Q_{\rm II}| < Q_{\rm I}$ always exists, while the solution with $|Q_{\rm II}| > Q_{\rm I}$ exists only when $d > d^*$. This agrees with the intuition that $Q_{\rm I}$ can be infinitely large to achieve the symmetric collision avoidance trajectory, but it must be greater than a certain value to ensure a collision avoidance with $r > r_s$. When $d < d^*$, the minimum acceptable value of $Q_{\rm I}$ is still greater than corresponding $|Q_{\rm II}|$ as predicted by Theorem 3, thus the solution with $|Q_{\rm II}| > Q_{\rm I}$ does not exist in this situation. Another important aspect is that if $d < d^*$, the solution with $Q_{\rm I} = |Q_{\rm II}|$ is the L_∞ optimal charge solution; when $d > d^*$, the circular transfer orbit is the L_∞ charge optimal solution. This helps to choose a proper value of $Q_{\rm I}$ such that the maximum charge level during the whole process is minimized.

Note that the criteria in Eq. (61) has exactly the same form as Eq. (42) in Reference 15. That equation is the requirement for the charge product such that the collision can be avoided. It has the same form as Eq. (61)

because the authors of Reference 15 assume that the two spacecraft are fully charged to get the criteria in Eq. (42). This assumption matches with the situation in Phase I, where the two spacecraft have a constant charge product and are repeling each other. The physical meanings of the criteria in Eq. (42) in Reference 15 can also be utilized here. For a given formation flying mission in which the maximum magnitude of the possible separation distance rate has been determined, Eq. (61) provides a guide to design the spacecraft charge devices such that $Q_{\text{I,c}}$ is achieveable, thus the collision can be avoided with a symmetric trajectory.

If the maximum charge product has been specified, then Eq. (63) below tells us the maximum allowable relative velocity that guarantees the collision to be avoidable.

$$v_0 \leq \sqrt{\frac{2Q_{\text{I,max}}k_c(m_1+m_2)}{m_1m_2}\frac{r_s(r_o-r_s)}{r_o(d^2-r_s^2)}} \tag{63}$$

Note that the inequality in Eq. (63) is obtained by solving for v_0 from the inequality in Eq. (61).

NUMERICAL SIMULATIONS

A numerical iteration routine using Newton's method to solve for a symmetric patched conic section trajectory has been setup. The logic of the routine is to search an appropriate time value t_B such that the target function $g(t_B)$ defined in Eq. (49) converges to zero, and the point D is the periapsis of Phase II.

The following numerical simulation cases show the effectiveness of the routine in different situations. All the cases share a common set of the parameters of the two spacecraft system:

$$m_1 = m_2 = 50\text{kg}, \quad r_o = 15\text{m}, \; r_s = 7\text{m}, \quad \gamma = 1. \tag{64}$$

The initial inertial state vectors are also the same across all numerical studies unless specified:

$$\begin{cases} \boldsymbol{R}_1(t_0) = [0,0,0]^T\text{m} \\ \boldsymbol{R}_2(t_0) = [-16,3,0]^T\text{m} \end{cases} \qquad \begin{cases} \dot{\boldsymbol{R}}_1(t_0) = [0,0,0]^T\text{m/s} \\ \dot{\boldsymbol{R}}_2(t_0) = [0.02,0,0]^T\text{m/s} \end{cases} \tag{65}$$

The numerical simulation integrates the fundamental equations of motion in Eq. (4) using a variable step size 4^{th} order Runge-Kutta integrator.

Ideal Conditions Examples

The phrase "ideal conditions" means the two spacecraft are flying in free space in a vacuum (no plasma environment) with $\lambda_d = \infty$. Setting the variable $\mu_{\text{I}} = -0.01\text{m}^3/\text{s}^2$, the corresponding charge product is $Q_{\text{I}} = 27.81\mu\text{C}^2$. Figure 9 shows two simulation results under these conditions. The first trajectory (solid line) has the point D as the periapsis of Phase II. The second trajectory (dashed line) is the case that the point D is the apoapsis of Phase II. This can be achieved by initializing t_B to be larger than $t_{p,\text{I}}$, and using $\mu_{\text{II}}^{(1)}$ instead of $\mu_{\text{II}}^{(2)}$ in the routine. Table 1 shows some detailed results of the simulations.

Table 1. Results of the ideal simulations.

	t_B [s]	r_D [m]	Q_{II} [μC^2]
sim 1	291.42	7.00	-6.480
sim 2	391.61	15.64	-1.036

In both of the two simulations the collision avoidance requirement $r_{\min} \geq r_s$ is satisfied, and the final relative speed direction is held the same as the initial direction. The first simulation has the shorter path, though the magnitude of Q_{II} is bigger. The apoapsis case (means the case with the poind D being the apoapsis of Phase II) is a conservative trajectory far exceeding the collision avoidance requirement. Noticing that a small difference in t_B results in a huge difference in the total maneuver time. The longer transition time span makes the apoapsis case much more vulnerable to disturbances.

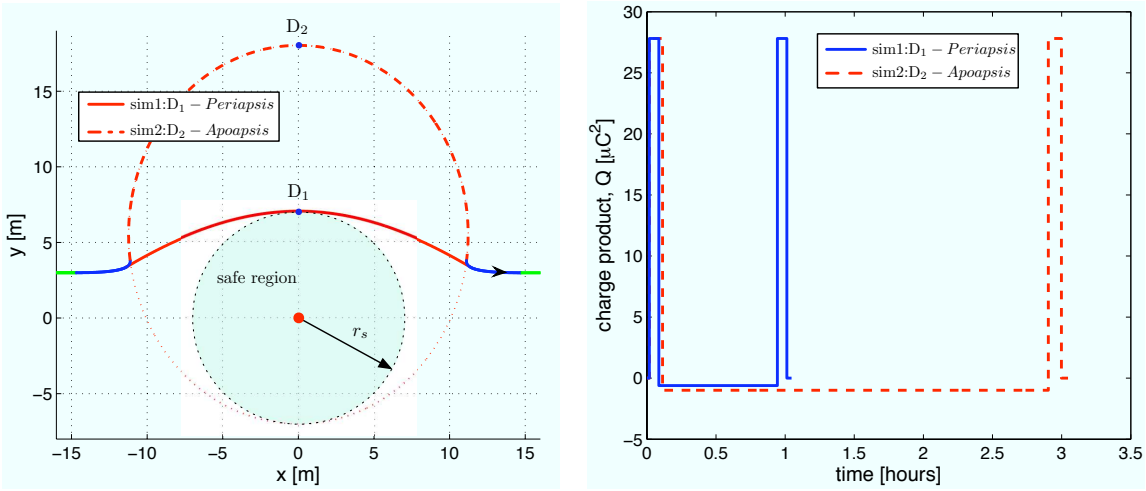

(a) Relative trajectories.

(b) Charge product histories.

Figure 9. Idea simulation.

Charge Expense Analysis

In these simulations the charge expense under for different choices of the free variable μ_{I} is analyzed. Two charge cost functions are defined as:

$$J_1 = \max(Q_{\text{I}}, |Q_{\text{II}}|), \qquad J_2 = \frac{2t_B Q_{\text{I}} + t_{\text{II}}|Q_{\text{II}}|}{2t_B + t_{\text{II}}} \tag{66}$$

Here J_1 is the maximum magnitude of the charge products. This is important when the maximum vehicle voltage level is of concern. J_2 is the time averaged charge product which provides insight into the nominal charge and voltages levels. Numerical sweeps on $|\mu_{\text{I}}|$ are performed using the same parameters as in Eq. (64), but with the different initial conditions:

$$\begin{cases} \boldsymbol{R}_1(t_0) = [0,0,0]^T \text{m} \\ \boldsymbol{R}_2(t_0) = [-16,6,0]^T \text{m} \end{cases} \qquad \begin{cases} \dot{\boldsymbol{R}}_1(t_0) = [0,0,0]^T \text{m/s} \\ \dot{\boldsymbol{R}}_2(t_0) = [0.03,0,0]^T \text{m/s} \end{cases} \tag{67}$$

Note that with the provided parameters and initial conditions, the condition in Theorem 3 is not satisfied, which implies the solution with $|Q_{\text{II}}| > Q_{\text{I}}$ exists. Figure 10 shows the values of J_1 and J_2 for each value of $|\mu_{\text{I}}|$. Figure 10(a) shows that the minimum value of J_1 is achieved at the marked point where $Q_{\text{I}} = |Q_{\text{II}}|$. As $|\mu_{\text{I}}|$ increases, before it reaches the point where $|Q_{\text{II}}| = Q_{\text{I}}$, $|Q_{\text{II}}|$ dominates and $J_1 = |Q_{\text{II}}|$. After the marked point, J_1 is linearly increasing because now $J_1 = Q_{\text{I}}$ and Q_{I} is proportional to $|\mu_{\text{I}}|$. Figure 10(b) shows that the minimum J_2 happens at the point where Q_{I} is minimum. This is because when $Q_{\text{I}} = Q_{\text{I},c}$, $2t_B$ is about two times greater than t_{II}, and as $|\mu_{\text{I}}|$ increases, t_B is increasing and t_{II} is decreasing. So the influence of t_B dominates J_2. Thus $J_2 \approx Q_{\text{I}}$ as shown in Figure 10(b).

The two plots in Figure 10 together show an example that according to difference charge expense concerns, the "optimal" solutions can be different.

Simulation With Debye Length Effect

The algorithm developed in this paper is an open loop programming algorithm, assuming that the spacecraft are flying in free space which implies the orbital motion and the Debye shielding effect haven't been taken into account.Figure 11 compares an ideal trajectory (dashed line) with a trajectory in the presence of the

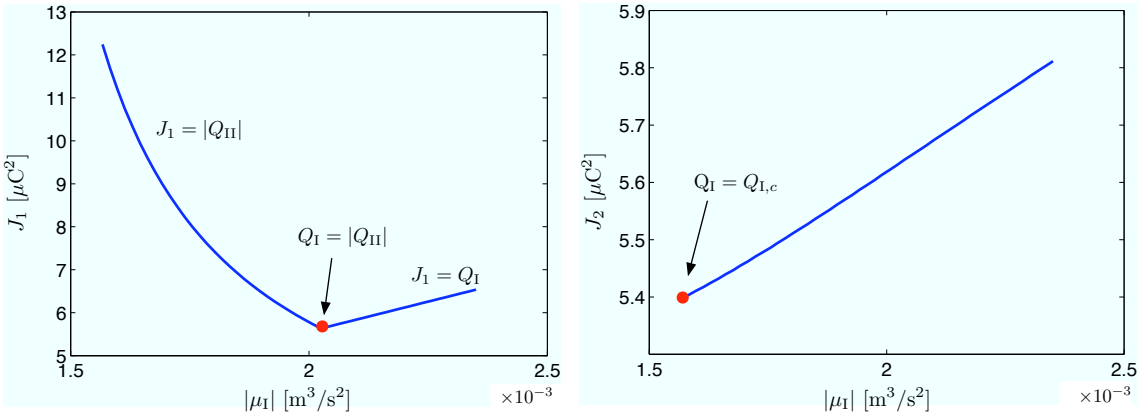

(a) Maximum charge product magnitude.

(b) Time averaged charge product.

Figure 10. Charge expense history while sweeping μ_I.

Debye shielding (solid line) under the same initial conditions. In the case that the Debye shielding is applied, the Debye length is set to be $\lambda_d = 50$m. This value represents the Debye length in deep space at 1 AU distance from the sun.

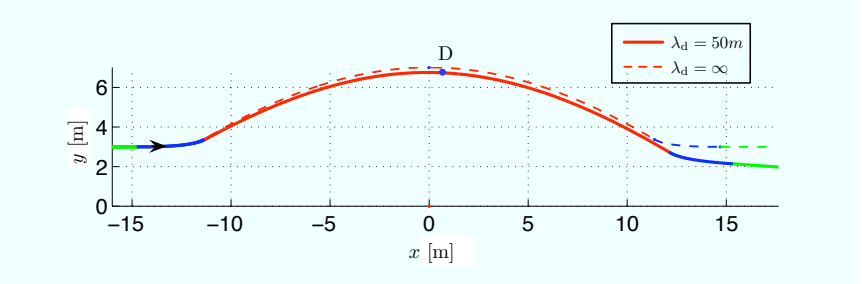

Figure 11. Relative trajectories of the two spacecraft under the condition $\lambda_d = 50$m.

The final velocity direction of the disturbed trajectory has an offset of 3.98° from the ideal trajectory. The minimum distance of the disturbed trajectory is 0.254m or about 3.6% less than that of the ideal case γr_s, due to the partial shielding of Coulomb force. The Debye length always decreases the effectiveness of the Coulomb repulsion. This effect could be compensated for with a $\gamma > 1$ safety factor. Future work will investigate how to feedback stabilize such open-loop trajectories. A challenge here is the under-actuated nature of the Coulomb thrusting. Further, the momentum conservation makes it impossible to reverse the motion to compensate for an overshoot. Any feedback control development could try to bias the tracking errors to slightly undershoot the desired trajectory.

CONCLUSION

This paper proposes a symmetric 3-phase relative trajectory composed of patched conic sections as the collision avoidance trajectory. An analytical solution to circular transitional symmetric trajectory and a numerical routine to find general symmetric trajectory solutions are developed. Under ideal conditions that no external forces act on the system and no Debye shielding exists, both of these two approaches generate a symmetric collision avoidance trajectory while preserving the initial relative velocity of the two spacecraft. With the presence of the Debye shielding effect, the trajectory deviates from the ideal trajectory, but only with small errors of a few percent. The results in this paper can be extended to more general applications

such as asymmetric flyby maneuver. The final relative velocity's direction can be controlled by changing the symmetric axis. The magnitude of the final relative velocity can be controlled by changing the energy level of Phase III, correspondingly the properties of Phase III trajectory are also changed and need to be treated carefully.

REFERENCES

[1] R. P. Patera and G. E. Peterson, "Space Vehicle Maneuver Method to Lower Collision Risk to an Acceptable Level," *Journal of Guidance, Control, and Dynamics*, Vol. 26, March–April 2003, pp. 233–237.

[2] G. L. Slater, S. M. Byram, and T. W. Williams, "Collision Avoidance for Satellites in Formation Flight," *Journal of Guidance, Control, and Dyanmics*, Vol. 29, Sept.-Oct. 2006, pp. 1140–1146.

[3] R. P. Patera, "Space Vehicle Conflict-Avoidance Analysis," *Journal of Guidance, Control, and Dynamics*, Vol. 30, March–April 2007, pp. 492–498.

[4] L. B. King, G. G. Parker, S. Deshmukh, and J.-H. Chong, "Spacecraft Formation-Flying using Inter-Vehicle Coulomb Forces," tech. rep., NASA/NIAC, January 2002. `http://www.niac.usra.edu`.

[5] K. Torkar, W. Riedler, and C. P. Escoubet, "Active Spacecraft Potential Control for Cluster – Implementation and First Results," *Annales Geophysicae*, Vol. 19, No. 10/12, 2001, pp. 1289–1302.

[6] K. Torkar and et. al., "Spacecraft Potential Control aboard Equator-S as a Test for Cluster-II," *Annales Geophysicae*, Vol. 17, 1999, pp. 1582–1591.

[7] D. R. Nicholson, *Introduction to Plasma Theory*. Krieger, 1992.

[8] T. I. Gombosi, *Physics of the Space Environment*. Cambridge University Press, 1998.

[9] C. C. Romanelli, A. Natarajan, H. Schaub, G. G. Parker, and L. B. King, "Coulomb Spacecraft Voltage Study Due to Differential Orbital Perturbations," *AAS Space Flight Mechanics Meeting*, Tampa, FL, Jan. 22–26 2006. Paper No. AAS-06-123.

[10] V. Lappas, C. Saaj, D. Richie, M. Peck, B. Streeman, and H. Schaub, "Spacecraft Formation Flying and Reconfiguration with Electrostatic Forces," *AAS/AIAA Space Flight Mechanics Meeting*, Sedona, AZ, Jan. 28–Feb. 1 2007. Paper AAS 07–113.

[11] H. Schaub and I. I. Hussein, "Stability and Reconfiguration Analysis of a Circulary Spinning 2-Craft Coulomb Tether," *IEEE Aerospace Conference*, Big Sky, MT, March 3–10 2007.

[12] H. Vasavada and H. Schaub, "Analytic Solutions for Equal Mass 4-Craft Static Coulomb Formation," *AAS/AIAA Astrodynamics Specialists Conference*, Mackinac Island, MI, Aug. 19–23 2007. Paper AAS 07–268.

[13] S. Wang and H. Schaub, "1-D Constrained Coulomb Structure Stabilization With Charge Saturation," *AAS/AIAA Astrodynamics Specialists Conference*, Mackinac Island, MI, Aug. 19–23 2007. Paper AAS 07–267.

[14] I. I. Hussein and H. Schaub, "Stability and Control of Relative Equilibria for the Three-Spacecraft Coulomb Tether Problem," *AAS/AIAA Astrodynamics Specialists Conference*, Mackinac Island, MI, Aug. 19–23 2007. Paper AAS 07–269.

[15] S. Wang and H. Schaub, "Spacecraft Collision Avoidance Using Coulomb Forces With Separation Distance Feedback," *AAS/AIAA Space Flight Mechanics Meeting*, No. Paper No. AAS 07-112, Sedona, Arizona, January 28–February 1 2007.

[16] S. Wang and H. Schaub, "Open-Loop Electrostatic Spacecraft Collision Avoidance Using Patched Conics Analysis," *AAS/AIAA Spaceflight Mechanics Meeting*, Galveston, TX, Jan. 27–31 2008. Paper AAS 08–207.

[17] I. I. Hussein and H. Schaub, "Invariant Shape Solutions of the Spinning Three Craft Coulomb Tether Problem," *AAS Space Flight Mechanics Meeting*, Tampa, Florida, January 22–26 2006. Paper No. AAS 06-228.

[18] J. A. Bittencourt, *Fundamentals Of Plasma Physics*. Springer-Verlag New York, Inc., 175 Fifth Avenue, New York, NY, 2004.

[19] H. Schaub, G. G. Parker, and L. B. King, "Challenges and Prospect of Coulomb Formations," *Journal of the Astronautical Sciences*, Vol. 52, Jan.–June 2004, pp. 169–193.

[20] H. Schaub and J. L. Junkins, *Analytical Mechanics of Space Systems*. Reston, VA: AIAA Education Series, October 2003.